Extension of cytomechanical analysis beyond the plane–strain approximation to 3D does not require fundamentally different experimental protocols. Our experiments already necessarily produce 3D image data in DIC through serial-focus image acquisition simply to make it possible to follow specimen shape changes and cell migration over time. The cross-correlation method for finding material displacements between sequential images can be implemented on 3D blocks of pixels in the same way as on 2D squares. Strain is computed no differently, except that $[e_{ij}]$ will generally be a 3×3 symmetric tensor rather than 2×2. Because the principal strains will then be represented as a triplet of scaled vectors at each grid point, and not as easily visualized graphically, new methods of display and quantification will be required. However, going to 3D analytical methods should greatly improve accuracy in identifying cytoskeletal structures and interpreting the observed pattern of strain in adjacent ECM.

Acknowledgments

We thank T. Brownlee and J. Airone for their experimental work in determination of Poisson's ratio; Dr. C. A. Otey for providing GFP–α-actinin expressing fibroblasts; D. Pane, M. Mantarro, and W. Galbraith for AIM software development; and A. Marciszyn for critical comments. This work was supported by Grants NIH AR-32461, NSF STC MCB-8920118, and NSF DBI-9987393.

[10] Measurements of Cell-Generated Deformations on Flexible Substrata Using Correlation-Based Optical Flow

By WILLIAM A. MARGANSKI, MICAH DEMBO, and YU-LI WANG

Introduction

The forces exerted by an adherent cell on the underlying substratum, the so-called cellular tractions, are important because of their potential involvement in cell motion, tissue morphogenesis, wound retraction, and in the transduction of information about the mechanical characteristics of the tissue.[1–4] Elastic substrate methods (ESMs) are the principal means for investigating the cellular tractions.

[1] C. G. Galbraith and M. P. Sheetz, *Curr. Opin. Cell Biol.* **10,** 566 (1998).
[2] D. P. Kiehart, C. G. Galbraith, K. A. Edwards, W. L. Rickoll, and R. A. Montague, *J. Cell Biol.* **149,** 471 (2000).
[3] A. Jacinto, A. Martinez-Arias, and P. Martin, *Nat. Cell Biol.* **3,** E117 (2001).
[4] C. Lo, H. Wang, M. Dembo, and Y.-L. Wang, *Biophys. J.* **79,** 144 (2000).

0076-6879/03 $35.00

The essential idea is to put a cell on a flexible substratum of known mechanical properties and to use the way this material deforms as the basis for drawing conclusions. All ESMs have three main components. The first deals with the fabrication and characterization of an appropriate elastic substratum and the culturing of cells onto this material. The second focuses on the experimental determination of the precise manner by which the substratum deforms under the action of adherent cells. Finally, the last component deals with the computational problem of interpreting the substrate deformations in terms of forces exerted by different regions of the cell.

A number of ESMs have been developed over the past 20 years, each with its advantages and disadvantages.[5] This article will focus on the application of polyacrylamide (PA) substrata that we developed.[4,6,7] The most significant advantages of PA substrata are their nontoxicity, mechanical stability, and ease of preparation. Furthermore, the mechanical stiffness of PA substrata can be tuned by varying the concentration of acrylamide or the crosslinker, while the chemical properties of the surfaces are determined by extracellular matrix proteins that are covalently linked. Methods for the preparation and physical characterization of PA substrata and the collection of cell and substrate images have been described in several publications.[8,9] Likewise the theory for the deformation of elastic substrata is well understood and the methodology to interpret such deformations in terms of cellular forces has been described previously.[10,11] Therefore, this article will focus exclusively on recent advances in the analysis of the determination of substrate deformations.

PA substrata are transparent and deformations are detectable only with the aid of (fluorescent) marker beads embedded within the elastic medium. In early applications, the motion of the substrate was determined by simple visual inspections. In this approach a pair of fluorescent images of the marker beads is recorded, one while the cell is adhered to the substratum (referred to as the "strained" image, I_1) and the other after the cell is removed by enzymatic or physical means (referred to as the "unstrained" image, I_0). Corresponding beads in the two images are identified visually and their coordinates are used for constructing displacement vectors. Unfortunately this simple approach breaks down catastrophically when motions are large compared to the spacing of the markers. This difficulty, known as the "correspondence problem," occurs because the observer becomes confused about the identification of corresponding beads in the strained and unstrained images.

[5] K. A. Beningo and Y.-L. Wang, *Trends Cell Biol.* **12,** 79 (2002).
[6] K. A. Beningo, M. Dembo, I. Kaverina, J. V. Small, and Y.-L. Wang, *J. Cell Biol.* **153,** 881 (2001).
[7] S. Munevar, Y.-L. Wang, and M. Dembo, *Biophys. J.* **80,** 1744 (2001).
[8] Y.-L. Wang and R. J. Pelham, *Methods Enzymol.* **298,** 489 (1998).
[9] K. A. Beningo, C.-L. Lo, and Y.-L. Wang, *Methods Cell Biol.,* **69,** 325 (2002).
[10] M. Dembo and Y.-L. Wang, *Biophys. J.* **76,** 2307 (1999).
[11] M. Dembo, T. Oliver, A. Ishihara, and K. Jacobson, *Biophys. J.* **70,** 2008 (1996).

To overcome the correspondence problem we have adapted an approach that is well known in a number of image analysis problems, namely correlation-based optical flow.[12,13] Essentially one defines a small patch in I_0 that contains a number of markers and then searches in I_1 for patches with a similar characteristic pattern of pixel intensities. The correspondence problem is alleviated because instead of following the motion of a single marker, one follows the collective motion of uniquely recognizable marker groupings. The end result is a robust estimate of the substrate deformation, usually accurate to within a pixel. This estimate can be refined by automatic procedures for the correction of image registration errors, and by detection/correction of physically improbably modes of deformation. Finally interpolation methods can be used to obtain true subpixel accuracy. Software implementing this algorithm on Linux workstations is available from the authors.

Correlation-Based Optical Flow

We will start with the images I_0 and I_1 that show the distribution of fluorescent markers in the unstrained and strained substrate. These images are loaded into computers as large matrices of n_x columns by n_y rows:

$$I_k \equiv \begin{bmatrix} P_k(1,1) & P_k(2,1) & \cdots & P_k(n_x-1,1) & P_k(n_x,1) \\ P_k(1,2) & P_k(2,2) & \cdots & P_k(n_x-1,2) & P_k(n_x,2) \\ \vdots & \vdots & \vdots & \vdots & \vdots \\ P_k(1,n_y) & P_k(1,n_y) & \cdots & P_k(n_x-1,n_y) & P_k(n_x,n_y) \end{bmatrix} \tag{1}$$

where the subscript $k = 0$ or 1 and $P_k(x, y)$ is the intensity at the pixel (x, y). Before further processing of these arrays, a constant is subtracted from all the P_k so that the average pixel intensity in both I_1 and I_0 is equal to zero.

Suppose that (x, y) and (u, v) are the coordinates of certain pixels in I_0 and I_1 respectively, and that we wish to test the possibility that the motion of the substratum has carried (x, y) onto (u, v). This requires that we construct two regions (the "correlation windows") that extend for a distance of C pixels from the central locations of (x, y) and (u, v), respectively. If B_0 is the region surrounding (x, y) and B_1 the region surrounding (u, v), then we may say that these regions have similar "intensity patterns" if the pixel at $(x + \delta_x, y + \delta_y)$ in B_0 has an intensity that is in some sense "close" to the intensity of the homologous pixel located at $(u + \delta_x, v + \delta_y)$ in B_1. Mathematically the image similarity in B_0 and B_1 can be measured in a variety of ways and careful systematic comparisons of the cost and efficiency of different approaches have been reported.[14] In the case of typical

[12] P. Anandan, *Int. J. Comput. Vision* **2,** 283 (1989).

[13] B. Jähne, "Digital Image Processing: Concepts, Algorithms, and Scientific Applications," 4th Ed. Springer Press, Berlin, Germany, 1997.

[14] J. L. Barron, D. L. Fleet, and S. S. Beauchemin, *Int. J. Comput. Vision* **12,** 43 (1994).

fluorescent images of substrata, which have a very high contrast, our results indicate that the optimal similarity measure is the so-called normalized cross-correlation coefficient:

$$R(x, y, u, v, C) \equiv \frac{\sum_{\delta_x}\sum_{\delta_y} P_0(x+\delta_x, y+\delta_y)P_1(u+\delta_x, v+\delta_y)}{\left(\sum_{\delta_x}\sum_{\delta_y} P_0^2(x+\delta_x, y+\delta_y)\right)^{1/2}\left(\sum_{\delta_x}\sum_{\delta_y} P_1^2(u+\delta_x, v+\delta_y)\right)^{1/2}} \quad (2)$$

The summations in this expression all range over the values δ_x and δ_y within the correlation windows of B_0 and B_1 (this means that δ_x and δ_y run between the limits of $-C$ and $+C$ except at locations close to the edges of an image).

This normalized cross-correlation has several properties that make it particularly suited as a measure of similarity in the current application. First, it can be shown that $R(x, y, u, v, C)$ falls in the range between -1 and $+1$ and that it approaches the upper limit only if $P_1(u+\delta_x, v+\delta_y)$ is equal to a positive constant times $P_0(x+\delta_x, y+\delta_y)$ for all choices of δ_x and δ_y. Similarly, $R(x, y, u, v, C)$ equals -1 only if $P_1(u+\delta_x, v+\delta_y)$ is equal to a negative constant times $P_0(x+\delta_x, y+\delta_y)$, i.e., if B_1 is the negative image of B_0. The function $R(x, y, u, v, C)$ is equal to 0 if the intensity patterns in B_0 and B_1 are completely uncorrelated. These properties mean that $R(x, y, u, v, C)$ is not affected by the linear rescaling of image intensity as might be caused by variations in the exposure time. Finally, constraining $R(x, y, u, v, C)$ to a range of -1 to $+1$ by normalization means that it has a comparable meaning regardless of the size and shape of the correlation windows. For these reasons the function $R(x, y, u, v, C)$ was clearly superior to the alternative approach of "sum of squared differences," and also slightly better than other measures of mutual variation within the regions B_0 and B_1.

Figure 1 shows typical examples of images I_0 and I_1. For aesthetic purposes each image is magnified so that the individual pixels can be discerned and in addition the intensities have been inverted so that the marker beads appear as black spots against a lighter background. Also illustrated is a correlation window in I_0 that is centered at the point (x, y) and that can be taken as a fixed reference. We also show two possible correlation windows in I_1. The first of these (shown with dashed outline) is centered at the same absolute image location as the reference window [i.e., $(u, v) = (x, y)$]. Because the substratum has moved, the features enclosed are quite dissimilar. The second window in I_1 (shown with solid outline) has been translated to a new location with center (u^*, v^*) such that $R(x, y, u, v, C)$ is maximized. The vector from the center of the dashed window to the center of the solid window gives a good estimate of the local substrate motion.

Among various parameters in correlation-based optical flow, the size of the correlation window C is of the utmost importance. Its value must be matched

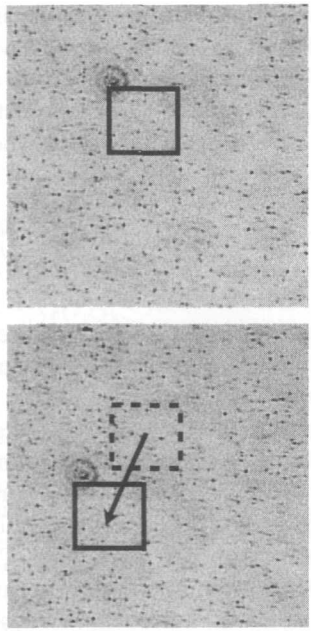

FIG. 1. Correlation-based optical flow. The basic premise is to compare pixel intensity patterns between two images, I_0 and I_1, to compute a motion field. The method begins by defining a reference window in I_0 (denoted by a solid outline). Then analogous patches within I_1 are examined, starting with a window (denoted by a dotted outline) centered at the exact pixel coordinates as the reference window. After finding the window (denoted by a solid outline) within I_1 that has an intensity pattern most similar to the reference window, a displacement vector is constructed that originates at the center of the dotted square and terminates at the center of the solid square. This vector gives an estimate of the local substrate motion.

by trial and error with the density of the marker beads. Too small a size would result in the inclusion of too few markers within the correlation window to form an unambiguous pattern, and the search for a matching pattern in I_1 will fail catastrophically. Too large a size would result in the loss of resolution since any differential movements within the correlation windows are neglected during the calculation of the cross-correlation coefficient.

Local Search Implementation

The ESM requires information about the substrate motion not at a single isolated point but throughout a large region surrounding a cell of interest. Generally it is neither necessary nor desirable to determine the movement at each pixel within this region, but only at nodes of a simple $m_x \times m_y$ lattice whose coordinates are expressed as (x_j, y_k) where $j = 1, 2, \ldots, m_x$ and $k = 1, 2, \ldots, m_y$. Once this lattice

is established, the next task is to determine the substrate displacement at each lattice node to within integer precision. This means we have to form a correlation window B_0 surrounding each of the points (x_j, y_k) in I_0 and find corresponding integer pixel coordinates (u^*_{jk}, v^*_{jk}) in I_1 by testing correlation windows B_1 at various positions (u, v) in I_1 and determining the position where $R(x_j, y_k, u, v, C)$ is maximized. The maximum value of the cross-correlation at a given lattice site is denoted by R^*_{jk}.

A straightforward and efficient method for finding (u^*_{jk}, v^*_{jk}) is to perform an iterative search. In this approach, one starts with an initial estimate of the position in I_1 where $R(x_j, y_k, u, v, C)$ is maximized, $(u^{(0)}_{jk}, v^{(0)}_{jk})$. If no better guess is available then this is simply taken to be the point (x_j, y_k), (i.e., assume there was no displacement at this location). One then computes the values of $R(x_j, y_k, u, v, C)$ for all pixels within some distance S from $(u^{(0)}_{jk}, v^{(0)}_{jk})$. The pixel with the maximal $R(x_j, y_k, u, v, C)$ then becomes a new estimate of the target position, $(u^{(1)}_{jk}, v^{(1)}_{jk})$. If this new estimate remains the same as the old estimate, then $(u^*_{jk}, v^*_{jk}) = (u^{(1)}_{jk}, v^{(1)}_{jk})$ and the procedure terminates; otherwise we continue the search.

This iterative method converges to the correct answer in most cases but it may be subject to error if the search distance S is too small. The distance S therefore needs to be adjusted by trial and error. Although the chance of making an error can be minimized by using a large S, this is expensive since the computational work increases as S^2. Fortunately, this problem is generally avoided because the substrate deformations are being determined at a large number of locations and because these motions are known to be a continuous function of the position. An efficient search strategy is to first determine (u^*_{jk}, v^*_{jk}) on a sparse lattice and with a large value of S. The density of the lattice and the value of S are then progressively increased and decreased, respectively. With each refined lattice the displacement of the nearest lattice point on the previous sparse lattice is used as the starting estimate. Because the starting values derived in this way are already quite accurate, the algorithm will usually converge to the target point in a single iteration, even if the search radius is only a few pixels.

Subpixel Resolution

The behavior of $R(x_j, y_k, u, v, C)$ in regions near the global optimum (u^*_{jk}, v^*_{jk}) for an example optical flow computation is illustrated in Fig. 2. The function has a well-defined maximum, $R^*_{jk} \approx 0.93$, and is quite high at pixels immediately surrounding (u^*_{jk}, v^*_{jk}) (the range is between 0.84 and 0.90). Moreover, even at distances up to two pixels away from the maximum the cross-correlation coefficient remains significantly elevated above the background. This remarkable smoothness and continuity of $R(x_j, y_k, u, v, C)$ near a point of optimal correlation is a general behavior, reflecting the fact that the image of a marker particle has a diffraction limited diameter of 0.3–0.6 μm while pixels are generally 0.1–0.3 μm

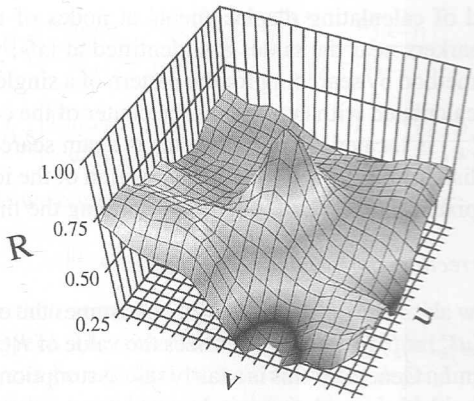

FIG. 2. Landscape of the cross-correlation coefficient around the global optimum. For fixed (x_j, y_k) in I_0, the cross-correlation coefficient $R(x_j, y_k, u, v, C)$ is plotted for various values of u and v in the neighborhood of the global optimum (u^*_{jk}, v^*_{jk}). As illustrated, $R(x_j, y_k, u, v, C)$ attains a well-defined maximum of $R^*_{jk} = 0.93$, but is still elevated well above the background even at distances ± 2 pixels away from the optimum. Thus, the cross-correlation coefficient is a smooth and continuous function of position and interpolation can be used to locate its optimum with subpixel accuracy.

in dimension. Therefore, the intensity of individual markers overlaps for a finite distance, within which the value of $R(x_j, y_k, u, v, C)$ changes only slightly.

We can exploit the smoothness and continuity of $R(x_j, y_k, u, v, C)$ to obtain a subpixel determination of the substrate motion using interpolation. After trying several schemes, we found that the simple five-point quadratic method is the most robust in real practice. This yields the following refined estimates for the coordinates of the maximum of $R(x_j, y_k, u, v, C)$:

$$u^{**}_{jk} = u^*_{jk} + \frac{0.5[R(x_j, y_k, u^*_{jk}+1, v^*_{jk}, C) - R(x_j, y_k, u^*_{jk}-1, v^*_{jk}, C)]}{2R(x_j, y_k, u^*_{jk}, v^*_{jk}, C) - R(x_j, y_k, u^*_{jk}-1, v^*_{jk}, C) - R(x_j, y_k, u^*_{jk}+1, v^*_{jk}, C)} \tag{3a}$$

$$v^{**}_{jk} = v^*_{jk} + \frac{0.5[R(x_j, y_k, u^*_{jk}, v^*_{jk}+1, C) - R(x_j, y_k, u^*_{jk}, v^*_{jk}-1, C)]}{2R(x_j, y_k, u^*_{jk}, v^*_{jk}, C) - R(x_j, y_k, u^*_{jk}, v^*_{jk}-1, C) - R(x_j, y_k, u^*_{jk}, v^*_{jk}+1, C)} \tag{3b}$$

This interpolation yields accuracy to approximately 0.1 pixel in ideal circumstances, where the correlation window undergoes motion with little internal deformation (see test results reported below).

If there are significant differential movements within the correlation window, then the displacement determined by interpolation may deviate slightly from the exact displacement at each marker particle. In this case a refined strategy has been

developed. Instead of calculating displacements at nodes of a simple lattice in I_0, well-defined markers near the nodes are identified at $(x_{j'}, y_{k'})$ (again using a correlation-based method by searching for the pattern of a single marker). The displacement is then calculated with $(x_{j'}, y_{k'})$ as the center of the correlation window B_0. Once $(u^*_{j'k'}, v^*_{j'k'})$ is located, a single marker is again searched for within the radius of an Airy disk from $(u^*_{j'k'}, v^*_{j'k'})$ and the position of the identified marker is determined at subpixel precision and is used for defining the final displacement.

Detecting and Correcting Correspondence Failures

The optical flow algorithm as described above assumes the existence of unique pixel coordinates $(u^{**}_{jk}, v^{**}_{jk})$ in I_1 that maximizes the value of $R(x_j, y_k, u, v, C)$ for any given (x_j, y_k) in I_0. Generally, this is a fairly safe assumption because there will be many markers inside the correlation window and the chances of two correlation windows having an identical marker distribution is low. However, despite the best efforts there is still a finite chance that a wrong assignment can occur at a small number of lattice sites. This correspondence failure can happen if the radius of the correlation window is small, the density of markers in the substrate is low, the signal-to-noise (S/N) ratio of the images is poor, or if the substrate displacements are very large. The algorithm can also fail if there is some feature in I_0 that is completely absent in I_1, for example, when autofluorescence of the cell or specks of dust appear in the image of marker particles. These problems cause the local search algorithm to yield artifactual results at the sites in question.

The general approach to avoid these correspondence failures is to look for suspicious displacements and to remove or recalculate them. A simple screen for correspondence failure is to calculate the S/N within the correlation window B_0 for each (x_j, y_k) and to treat the node as suspicious if the S/N falls below a defined threshold. Alternatively, correspondence failure can be detected by comparing the value of $R(x_j, y_k, u, v, C)$ at each (u^*_{jk}, v^*_{jk}) against a defined threshold. Clearly if this maximal $R(x_j, y_k, u, v, C)$ is close to 0, the match between B_0 and B_1 must be treated as highly suspicious.

A more sophisticated screen takes into account the physical characteristics of the displacements of an elastic substrate. These displacements are continuous functions of position, whereas correspondence failures generally result in discontinuous, random displacements and can usually be detected by checking the relationship among the magnitude of neighboring displacements. To be specific, at a lattice node (x_j, y_k) we estimate the magnitudes of the so-called "in-plane strain components" as follows:

$$\epsilon^2_{xx} = 0.5\left|\frac{u^{**}_{(j+1)k} - u^{**}_{jk}}{x_{j+1} - x_j} - 1\right|^2 + 0.5\left|\frac{u^{**}_{jk} - u^{**}_{(j-1)k}}{x_j - x_{j-1}} - 1\right|^2 \tag{4a}$$

$$\epsilon^2_{yx} = 0.5\left|\frac{v^{**}_{(j+1)k} - v^{**}_{jk}}{x_{j+1} - x_j}\right|^2 + 0.5\left|\frac{v^{**}_{jk} - v^{**}_{(j-1)k}}{x_j - x_{j-1}}\right|^2 \tag{4b}$$

$$\epsilon_{xy}^2 = 0.5\left|\frac{u_{j(k+1)}^{**} - u_{jk}^{**}}{y_{k+1} - y_k}\right|^2 + 0.5\left|\frac{u_{jk}^{**} - u_{j(k-1)}^{**}}{y_k - y_{k-1}}\right|^2 \tag{4c}$$

$$\epsilon_{yy}^2 = 0.5\left|\frac{v_{j(k+1)}^{**} - v_{jk}^{**}}{y_{k+1} - y_k} - 1\right|^2 + 0.5\left|\frac{v_{jk}^{**} - v_{j(k-1)}^{**}}{y_k - y_{k-1}} - 1\right|^2 \tag{4d}$$

Then for each node we compute the norm of the strain tensor:

$$\|\epsilon_{jk}\| = \sqrt{\epsilon_{xx}^2 + \epsilon_{yx}^2 + \epsilon_{xy}^2 + \epsilon_{yy}^2} \tag{5}$$

If $\|\epsilon_{jk}\|$ is greater than some limiting value $\epsilon_{\max}$, then the values of $(u_{jk}^{**}, v_{jk}^{**})$ are regarded as suspect. The exact value of the cutoff limit, $\epsilon_{\max}$, is generally on the order of 1 but can be adjusted by trial and error depending on the nature of the data and the preference of the user. After all nodes have been checked, the displacement at suspect nodes is recalculated. In this recalculation, however, the radius C of the correlation window is increased so as to reduce the chances of a second correspondence failure. In addition, we use the value of (u_{jk}^{*}, v_{jk}^{*}) from the closest nonsuspect node as the starting estimate $(u_{jk}^{(0)}, v_{jk}^{(0)})$ for the local search at these suspect nodes.

Correcting Image Registration Artifacts

Small movements of the substrate or microscope stage that occur in between the acquisition of I_1 and I_0 cause systematic displacement of all marker particles by a constant vector (d_x, d_y). This so-called "registration artifact" is superimposed on the actual physical displacements and needs to be corrected before any calculation of the cellular forces is attempted. This correction is possible because as long as the lattice covers a substantial area outside the cell, many of the nodes (x_j, y_k) will be far away from the cell and will have a displacement that is due only to the registration artifact. Consequently, a simple approach to remove the registration error is to define a correlation window B_0 in a reference region far away from the cell and to calculate the substrate displacement at this location. This displacement (d_x, d_y) is treated as the registration artifact and is subtracted from the subsequent calculations. The major drawback of this approach is that sometimes it is difficult to identify such a reference region due to possible displacements caused by neighboring cells outside the field of observation.

A more robust, nonbiased strategy is built upon the fact that the displacement of the registration artifact should occur with the maximal frequency. Therefore if one constructs a histogram of the number of nodes versus the distance of displacement, the peak should be located at (d_x, d_y). We devised an efficient "nested histogram algorithm" to carry out this task. The scheme is initiated by sorting the uncorrected x and y displacements into a finite number of bins. This generates two crude histograms for the x and y displacements, respectively. Figure 3a shows such a histogram along the x direction for a typical experiment. As can be seen, the

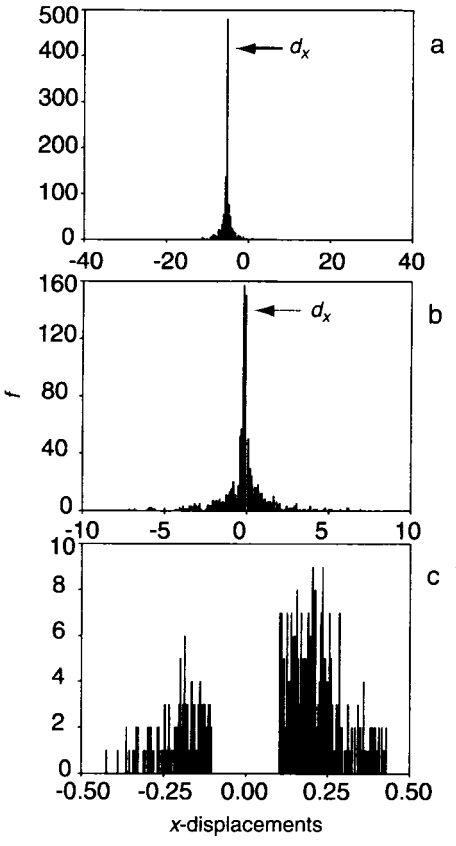

FIG. 3. Nested histogram algorithm. (a) A frequency distribution with a finite number of bins is created for the x displacements, $(u_{jk}^{**} - x_j)$. The center of the bin having the highest frequency (f) gives a first estimate of the most likely x displacement (d_x) of the substrate. The x coordinate of each node is then adjusted as $x_j = x_j + d_x$ so that the most frequent x displacement of the motion field will be the zero. (b) Finer correction of the registration artifact is performed by using the same number of bins while decreasing the interval size and then recomputing the histogram for the corrected x displacements, $[u_{jk}^{**} - (x_j + d_x)]$. (c) The process continues until the size of the interval or the maximum frequency becomes so small that a meaningful distribution cannot be generated. Note that the computation of the registration artifact in the y direction is completely analogous and, thus, is not shown here.

highest frequency occurs at $d_x \approx -4.0$ pixels. A second pair of histograms is then constructed, by centering at the most frequent displacement identified in the previous histogram and subdividing the bins to obtain a smaller interval and hence a higher resolution. As seen in Fig. 3b, the displacement with the highest frequency is now centered at $d_x \approx -0.5$ pixel. Combining the two corrections yield a net estimated registration artifact of $d_x \approx -4.5$ pixels. This process can be

iterated, by doubling or quadrupling the resolution at each iteration and summing the corrections, to obtain the desired resolution. In the present example the process terminated with the histogram shown in Fig. 3c.

Overview of Optical Flow Algorithm

For easy reference the following flowchart summarizes the correlation-based optical flow algorithm in its most basic form. Slight modifications might be necessary in some instances.

1. Load images I_0 and I_1 into the computer as integer matrices.
2. Choose lattice nodes (x_j, y_k) and parameters C, S, $\epsilon_{\max}$.
3. Subtract average intensity from each image.
4. For each lattice node (x_j, y_k) perform steps 5–10.
5. Estimate $(u_{jk}^{(0)}, v_{jk}^{(0)})$ using existing results from a sparse lattice or by setting them equal to (x_j, y_k).
6. Use the local search algorithm to compute (u_{jk}^{*}, v_{jk}^{*}) and R_{jk}^{*}.
7. Use quadratic interpolation Eqs. (3a and 3b) to compute $(u_{jk}^{**}, v_{jk}^{**})$.
8. Compute $\|\epsilon_{jk}\|$ using Eq. (5).
9. Set $C = 2C$ and recompute $(u_{jk}^{**}, v_{jk}^{**})$ if $\|\epsilon_{jk}\| > \epsilon_{\max}$.
10. Recompute $\|\epsilon_{jk}\|$ using Eq. (5).
11. Calculate the most likely substrate displacement (d_x, d_y) caused by registration artifacts using the nested histogram algorithm.
12. For all (j, k), set $(x_j, y_k) = (x_j + d_x, y_k + d_y)$.
13. For all (j, k), write x_j, y_k, u_{jk}^{**}, v_{jk}^{**}, R_{jk}^{*}, and $\|\epsilon_{jk}\|$ to a data file.
14. Stop.

Illustrative Results

In Figs. 4 and 5, we illustrate the performance of our algorithm by determining the substrate displacements produced by a NIH 3T3 cell adhering to a PA substratum coated with type I collagen. The substratum in this experiment was fabricated using 5% (w/v) acrylamide and 1% (w/v) bisacrylamide and had an estimated Young's modulus of 2.8×10^4 Pa and Poisson's ratio of 0.30. The substratum contained 0.20 visible markers per micrometer square of the surface. The raw images I_0 and I_1 were initially stored as 8-bit tiff files with [512 × 512] pixels. The final magnification was 0.30 μm/pixel.

Substrate displacements were first determined by the standard method using a lattice of 32 × 32 nodes and with parameters $C = 5$, $S = 5$, and $\epsilon_{\max} = 0.316$ (Fig. 4a). A small correlation window was deliberately utilized in this calculation, so that there were a significant number of correspondence failures that were corrected using step 9 of the algorithm. To identify these corrections, the threshold

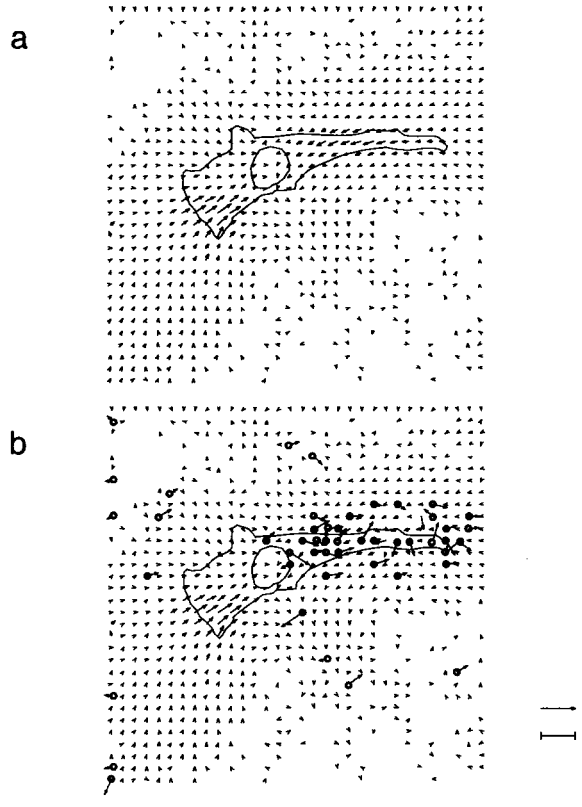

FIG. 4. Detecting and correcting suspect displacement vectors. A displacement field was computed on a lattice of 32×32 nodes with $C = S = 5$. The performance of the optical flow algorithm in detecting and correcting correspondence failures was studied by either setting $\epsilon_{max} = 0.316$ (a) or $\epsilon_{max} = 100$ (b). Lattice sites that were affected by changing ϵ_{max} in this way are indicated with small circles. The length scale represents 46.25 pixels and the displacement vectors are rendered at three times the actual motion for better visibility.

ϵ_{max} was reset to a very large value to bypass the corrections and the calculation was repeated (Fig. 4b). The lattice nodes in Fig. 4b where results were affected by the absence of any correspondence check are indicated by small circles. Clearly the check found all points where obvious problems occurred and there are very few if any false positives. We conclude that the check based on $\|\epsilon_{jk}\|$ and the recalculation with increased correlation radius is quite effective at detecting and correcting correspondence failures.

Figures 5 illustrates the removal of the registration artifact using our nested histogram algorithm. Using the same starting images described above, the substrate displacements were calculated on a lattice of 32×32 nodes with parameters $C = 10$, $S = 5$, and $\epsilon_{max} = 0.316$. In step 11 of the algorithm, the nested

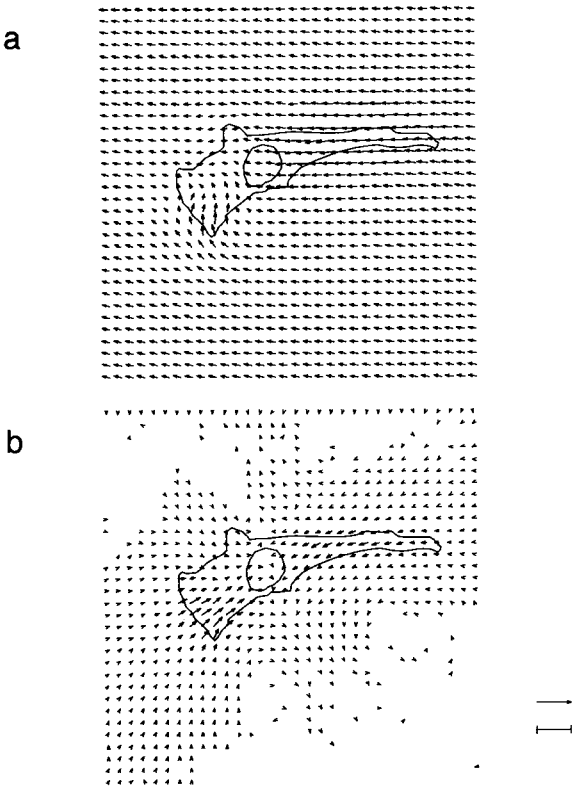

FIG. 5. Correcting image registration artifacts using the nested histogram algorithm. A displacement field was computed on a lattice of 32×32 nodes with $C = 10$, $S = 5$, and $\epsilon_{max} = 0.316$. The performance of the optical flow algorithm in correcting registration artifacts was tested by either omitting (a) or utilizing (b) step 12 of the algorithm. The length scale represents 46.25 pixels and the displacement vectors are rendered at three times the actual motion for better visibility.

histogram calculation indicated that the most likely substrate displacement was $\mathbf{d} = (-5.09, -0.83)$. Comparison of the results with (Fig. 5b) and without (Fig. 5a) the correction of registration artifact (step 12) indicates that the nested histogram method yields an excellent estimate of the registration artifact. The displacements observed give a much better representation of the action of the cell on the substratum.

As a simple empirical test of the overall accuracy of our optical flow algorithm, images of several standard PA substrata were recorded under conditions designed to simulate those of a typical experiment. After recording an initial image, the substratum was left on the microscope stage for 30 min before the second image was recorded. During this interval various sham procedures were implemented to replicate some standard procedures that might be involved in a real experiment

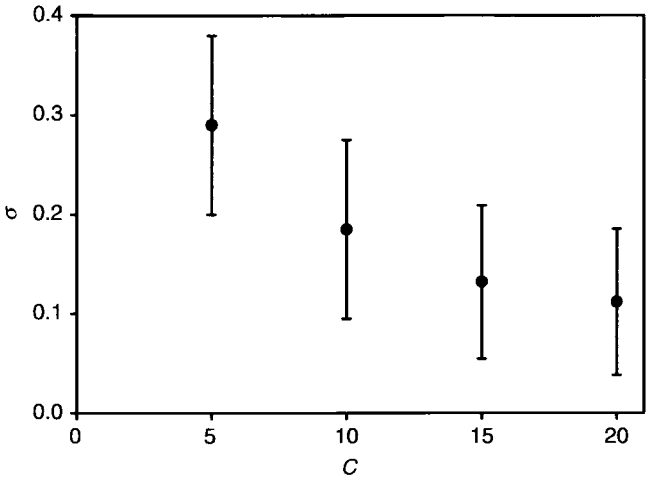

FIG. 6. Accuracy of computing substrate displacements vectors. A series of images of a cell-free, unstrained substrate were taken under conditions that simulated a real experiment. The motion between 30 image pairs was measured on a lattice of 100×100 nodes with $S = 5$, $\epsilon = 0.316$, and for values of C as indicated. The error $\sigma = \sqrt{\sigma_x^2 + \sigma_y^2}$ of the combined x and y motions was computed using all 10^4 lattice points. Each data point consists of the mean and standard deviation of σ. Results indicate that σ approaches ± 0.10 pixels when image quality is optimal.

(i.e., flushing and replacing the medium and purposely jostling the stage). The displacement field between two images was measured on a lattice of 100×100 nodes using parameters $S = 5$, $\epsilon_{\max} = 0.316$, and various sizes C of the correlation window. The mean of the registration magnitude in these experiments was $(\sqrt{(d_x)^2 + (d_y)^2})_{\text{ave}} \approx 3$ pixels, which is typical of real experiments. The residual systematic motion after the correction of the registration artifacts varied between 0.06 pixels at $C = 5$ and 0.03 pixels at $C = 20$. For each value of C, the error $\sigma = \sqrt{\sigma_x^2 + \sigma_y^2}$ of the combined x and y motions was computed using all 10^4 lattice nodes and the results for 30 pairs of images are shown in Fig. 6. Note that the error is about ± 0.30 pixels when $C = 5$, decreases to ± 0.19 pixels when $C = 10$, and approaches ± 0.10 pixels at very large C.

These analyses demonstrate that a small C causes an increase in correspondence failure and error, due to the insufficient number of beads in many of the correlation windows. As C increases, the error σ approaches an asymptotic value greater than zero because factors other than the correspondence problem are limiting. These other factors include the inaccuracy in the registration error and the interpolation error. The asymptotic value of σ in this ideal limit is on the order of ± 0.10 pixels. Similar accuracy in the measurement of uniform motion fields using optical flow under ideal circumstances has also been reported by

Seitz.[15] Of course, these results should be regarded as lower bounds of the errors in more realistic circumstances. In particular, if motion of the substratum is nonuniform, then σ values may double or even triple those found in this simple test.

Summary

The optical flow algorithm presented here is a robust method that rapidly yields a high-density field of substrate displacement vectors based on two optical images. We found that one of the limiting factors, at least for inexperienced experimentalists, is the consistency of focusing or the drift in microscope focus. However, with properly collected images the standard error of the measurement was estimated to be on the order of ± 0.10 pixels. Finally, although the discussion has been focused on the displacement of flexible substrata, a similar method should be applicable for detecting movements on other types of images, as long as the movement involves a certain degree of local coordination.

Acknowledgments

This research was supported by the Computational Science Graduate Fellowship funded by the Department of Energy to W. A. Marganski, NIH Grant GM61806 to M. Dembo, and NIH Grant GM32476 and NASA Grant NAG2-1495 to Y.-L. Wang.

[15] P. Seitz, *Opt. Eng.* **27,** 535 (1988).

[11] Single-Molecule Imaging of Rotation of F_1-ATPase

By KENGO ADACHI, HIROYUKI NOJI, and KAZUHIKO KINOSITA, JR.

Introduction

A single molecule of F_1-ATPase has been shown to be a rotary motor, driven by adenosine triphosphate (ATP) hydrolysis, in which the central γ subunit rotates against a surrounding cylinder made of alternately arranged three α and three β subunits.[1–5] Together with another (yet putative) proton-driven rotary motor F_0, it constitutes the F_0F_1-ATP synthase that synthesizes ATP from adenosine

[1] P. D. Boyer, *Biochim. Biophys. Acta* **1140,** 215 (1993).
[2] P. D. Boyer, *Biochim. Biophys. Acta* **1458,** 252 (2000).
[3] K. Kinosita, Jr., R. Yasuda, H. Noji, and K. Adachi, *Philos. Trans. R. Soc. Lond. B* **355,** 473 (2000).
[4] K. Kinosita, Jr., R. Yasuda, and H. Noji, *Essays Biochem.* **35,** 3 (2000).
[5] H. Noji and M. Yoshida, *J. Biol. Chem.* **276,** 1665 (2001).

0076-6879/03 $35.00